Available online at www.sciencedirect.com
ScienceDirect
Physics of the Earth and Planetary Interiors 159 (2006) 213–224
PHYSICS OF THE EARTH AND PLANETARY INTERIORS
www.elsevier.com/locate/pepi

Correlated shear and bulk moduli to 1400 km beneath the Mediterranean region

C. Schmid[a], S. van der Lee[b,*], D. Giardini[a]

[a] Institute of Geophysics, ETH Zürich, Switzerland
[b] Department of Geological Sciences, Northwestern University, Evanston, IL, USA

Received 30 March 2006; received in revised form 7 July 2006; accepted 12 July 2006

Abstract

We present a new model for the shear and compressional wave velocity structure of the Mediterranean plate boundary region. The model is obtained by a combined inversion of *S* and *P* data, where we solve in one single step for shear wave and bulk sound velocity variations. The ratios between the types of seismic velocities inferred from the combined inversion constrain the origin of heterogeneity. Our model is dominated by fast anomalies from subducted oceanic lithosphere. We found that only a slight amount of bulk sound velocity heterogeneity is required to explain the combined set of *P* and *S* data. Thus, compressional wave velocity anomalies are dominated by shear modulus heterogeneity and the ratio between bulk sound and shear wave velocity heterogeneity suggests a predominantly thermal origin.

Keywords: Mediterranean region; Seismic tomography; Mantle; Joint inversion

1. Introduction

The Mediterranean region contains the boundary between the African and the Eurasian plate. The plate boundary runs from the Azores triple junction to the triple junction with the Arabian plate. Present and past geodynamics of this region are complex and highly heterogeneous. Tectonic reconstructions for the region are provided by Dercourt et al. (1986) or Stampfli and Borel (2002), for example.

Previous models for the 3D heterogeneity in seismic velocity in the Mediterranean mantle are based on arrival time data of *P* or *S* body waves (Spakman et al., 1993; Piromallo and Morelli, 2003; Schmid et al., 2006; Bijwaard, 1999), dispersion measurements of surface waves (Panza et al., 1980; Pasyanos and Walter, 2002) and the inversion of waveforms of regional *S* and surface waves (Zielhuis and Nolet, 1994; Marone et al., 2004).

Typically, the *S* velocity models derived from arrival time data are not as well resolved as corresponding *P* models because the *S* data coverage is different from that for *P* due to the *S* data being fewer. These *S* data also have larger uncertainties than *P* arrival times, allowing *P* models to be better constrained. Wave train *S* velocity models have longer lateral resolution lengths, though better depth resolution in the shallow mantle, than *P* models, which are derived from arrival times. Wave train *S* models also have larger volumes of more uniform data coverage compared to *P* velocity models. These differences between *S* and *P* models hinder a quantitative comparison of *P* and *S* velocity models. However, advances in delay-time estimation (VanDecar and Crosson, 1990) and more recently in combining teleseismic *S* wave delay times with regional waveforms of

* Corresponding author. Tel.: +1 847 491 8183.
E-mail address: suzan@earth.northwestern.edu (S. van der Lee).

0031-9201/$ – see front matter © 2006 Elsevier B.V. All rights reserved.
doi:10.1016/j.pepi.2006.07.003

S and surface waves in a joint tomographic inversion (Schmid et al., 2006) is now producing S velocity images of comparable sharpness to P velocity images, allowing a more straightforward comparison of P and S velocity models.

Combined inversions of P and S data would be advantageous, since these can contribute to a deeper understanding on the nature of the velocity perturbations, aiding the discrimination between thermal and compositional heterogeneity. P velocity depends on bulk modulus (K), shear modulus (μ) and density (ρ), S velocity depends only on μ and ρ. It is not possible to extract individual perturbations of μ, K and ρ based on travel time data only. However, one can solve for perturbations in the ratios μ/ρ and K/ρ. The square root of the former is the shear wave velocity, while the square root of the latter is termed bulk sound velocity, despite the fact that no physical wave travels with this velocity.

On a global scale, joint inversions of P and S data for bulk sound and shear wave velocity heterogeneity were presented by Su and Dziewonski (1997), Kennett et al. (1998), Masters et al. (2000), Antolik et al. (2003), Gorbatov and Kennett (2003), Kennett and Gorbatov (2004). While these studies agree in their main findings, there are also some discrepancies. In the lower mantle, P wave velocity heterogeneity can be explained predominantly by variations in shear wave velocity with only small variations bulk sound velocity. While all report anti-correlation of bulk sound and shear wave velocity in the lowermost mantle, they differ on the degree and sign of correlation for the rest of the lower mantle. Kennett et al. (1998), Gorbatov and Kennett (2003), Kennett and Gorbatov (2004) further made the observation that stagnant slabs in the mid mantle show a pronounced fast anomaly in the bulk sound velocity with only faint shear wave velocity anomalies.

In this paper, we present the results of joint P and S inversions for bulk sound speed and shear wave velocity perturbations beneath the Mediterranean plate boundary region.

2. Theory

2.1. Travel time inversion

Classic teleseismic traveltime inversion (for a detailed treatment of the subject the reader is referred to Spakman et al. (1993), for example) is based on the traveltime equation, which is given by

$$\delta t \approx -\int_{L_0} \frac{1}{v_0}\frac{\delta v}{v_0}\mathrm{d}l \tag{1}$$

Discretization leads to a linear system of equations,

$$Am = d \tag{2}$$

where m is a vector with the unknown quantities, i.e. the spatial distribution of seismic velocity or its reciprocal, slowness. Vector d contains the measured data, i.e. arrival time delays, and matrix A contains the partial derivatives that relate m to d. In our application m consists of velocity perturbations, source relocation, source time adjustments and station statics. The velocity perturbations are linearly interpolated within triangles on spherical shells, as in Van der Lee and Nolet (1997).

To better localize velocity heterogeneity, we further add information from regional waveform data manner as described in Schmid et al. (2006), who demonstrated that the joint inversion of regional waveform data and phase arrival time data leads to a better constrained and resolved model, since the two complement each other optimally. The teleseismic body wave arrival time data have limited resolution in the depth direction at shallow levels (depths < 300 km) due to the nearly vertical direction of incidence. The regional waveform data on the other hand, start to loose resolution with increasing depth (>500 km). The purpose of the combined data set thus is to correct the teleseismic arrival time data for the shallow structure.

2.2. Separation into bulk and shear modulus perturbations

Compressional wave speed α is defined as

$$\alpha = \sqrt{\frac{K + (4/3)\mu}{\rho}} \tag{3}$$

while shear wave speed β is given by

$$\beta = \sqrt{\frac{\mu}{\rho}} \tag{4}$$

Thus, perturbations in shear modulus will affect the travel times of both P and S waves, while perturbations in the bulk modulus only affect P travel times.

The bulk sound speed, Φ, is defined as

$$\Phi = \sqrt{\frac{K}{\rho}} = \sqrt{\alpha^2 - \frac{4}{3}\beta^2} \tag{5}$$

Adding small perturbations,

$$\Phi \to \Phi + \delta\Phi; \quad \alpha \to \alpha + \delta\alpha; \quad \beta \to \beta + \delta\beta \tag{6}$$

and inserting these new values in Eq. (5) and neglecting second order terms gives:

$$\Phi\delta\Phi = \alpha\delta\alpha - \frac{4}{3}\beta\delta\beta \tag{7}$$

or

$$\delta\alpha = \frac{\Phi}{\alpha}\delta\Phi + \frac{4\beta}{3\alpha}\delta\beta \tag{8}$$

To invert for the the P structure, we solve a system of equations that contains lines of the type,

$$A_{i1}\delta\alpha_1 + A_{i2}\delta\alpha_2 + \cdots + A_{ij}\delta\alpha_j + \cdots = \delta t_i \tag{9}$$

The delay time for event i is a sum of the partial derivatives times the velocity perturbations at each node or cell j.

We can now insert Eq. (8) into the linear system of Eq. (9),

$$A_{ij}\delta\alpha_j = A_{ij}\left(\frac{\Phi_j}{\alpha_j}\delta\Phi_j + \frac{4\beta_j}{3\alpha_j}\delta\beta_j\right) \tag{10}$$

so that after some rearrangement the system becomes,

$$A_{i1}\left(\frac{\Phi_1}{\alpha_1}\right)\delta\Phi_1 + A_{i2}\left(\frac{\Phi_2}{\alpha_2}\right)\delta\Phi_2 + \cdots + A_{i1}\left(\frac{4\beta_1}{3\alpha_1}\right)\delta\beta_1 + A_{i2}\left(\frac{4\beta_2}{3\alpha_2}\right)\delta\beta_2 \cdots \tag{11}$$

where $A_{ij}(\Phi_j/\alpha_j) = A'_{\Phi ij}$ and $A_{ij}(4\beta_j/3\alpha_j) = A'_{\beta ij}$. The model vector now contains twice as many elements as when only inverting for P. Completing the

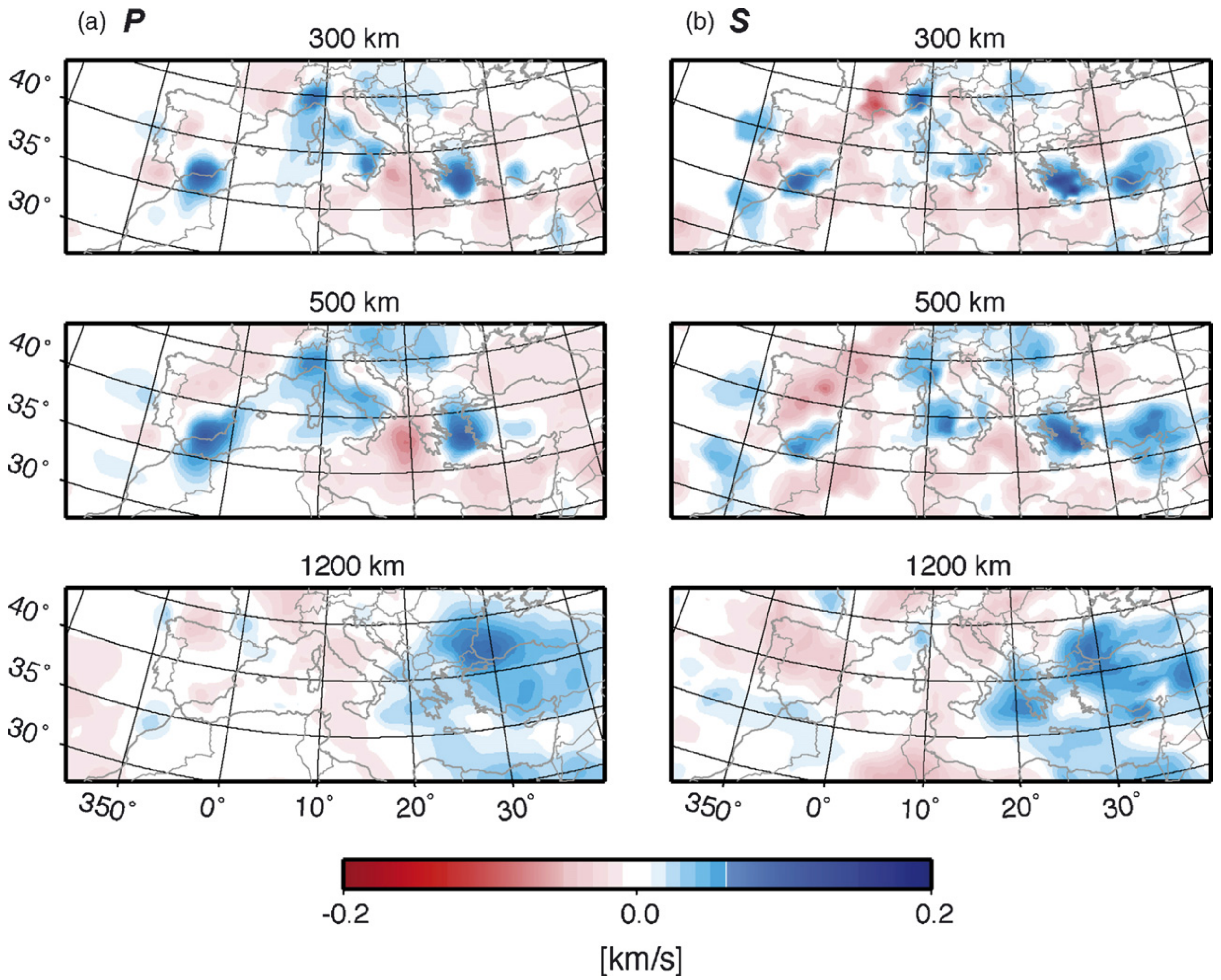

Fig. 1. Maps of P and S velocity heterogeneity obtained from separate inversions.

system of equations with the equations for S arrival times yields:

$$\begin{pmatrix} A_\beta & 0 \\ A'_\beta & A'_\Phi \end{pmatrix} \begin{pmatrix} m_\beta \\ m_\Phi \end{pmatrix} = \begin{pmatrix} d_S \\ d_P \end{pmatrix} \quad (12)$$

The system is mixed-determined and we add regularization equations (norm damping and first-difference damping) (VanDecar, 1991). We solve the system iteratively using conjugate gradients.

3. Data

We use relative arrival time data (Schmid et al., 2004), measured by using the multi channel cross-correlation method (MCCC) of VanDecar and Crosson (1990) applied to seismograms from MIDSEA (Van der Lee et al., 2001) and permanent stations in the Mediterranean region. Measuring by cross-correlation significantly increasing the number of useful S arrivals compared to traditional travel-time picking. To approximately equalize the number of S to that of P measurements, we measured S delay times through cross-correlating the S arrivals in a larger time window than used for P. Unlike Kennett et al. (1998), we do not restrict the data selection to common P and S ray-paths. We measured about ∼3000 delay times for each P and S. The P and S body wave coverage is very similar (Schmid et al., 2004), since the station setting is identical and there is an overlap in the events that were analyzed.

We use a modified iasp91 (Kennett and Engdahl, 1991) as background model, which has a thinner crust and lower velocities in the uppermost mantle in order to reflect the regionally averaged structure of the Eurasia-Africa plate boundary region (Marone et al., 2003).

We augmented the teleseismic delay time data set with the regional waveform data set assembled by Marone et al. (2004) and used in Schmid et al. (2006). It consists of regional Rayleigh waveform fits, including fundamental and higher modes, for 1136 seismograms, yielding a total number of 8714 surface-wave constraints. Since the sensitivity of the regional waveforms to the compressional wave velocity is rather weak and practically confined to the crust, we neglect it. The inclusion of regional waveform data, which are predominantly sensitive to the shear modulus, does tighten the depth distribution of the anomalies but does not affect the relation between bulk and shear heterogeneity we infer.

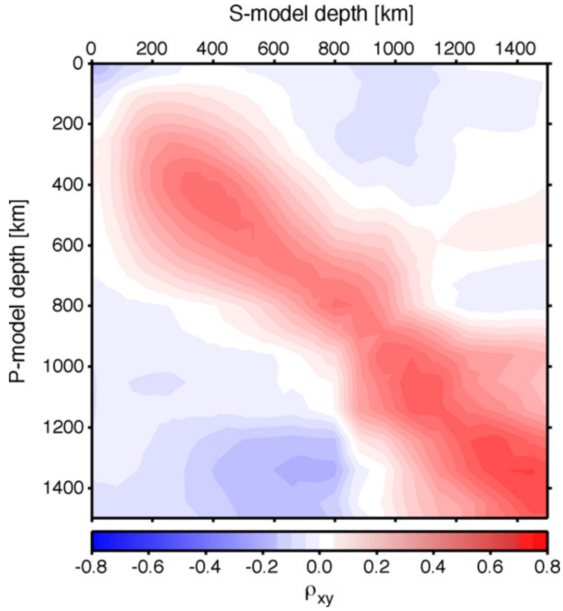

Fig. 2. Correlation matrix ρ between S and P models obtained from separate inversions. We use $\rho_{xy} = \mathrm{cov}(x, y)/\sigma_x\sigma_y$, where x and y are the depths in the P and S models, respectively, for which the correlation is calculated.

4. Results

4.1. Inversion of P and S data separately

Fig. 1 shows depth sections for separate, independent S and P inversions, using only the teleseismic arrival time data. The imaged patterns for P and S anomalies correlate (Fig. 2), which is expected since the P and S delay times are correlated as well (Schmid et al., 2004). Despite the great similarity of the two patterns, there are some notable differences. For example, beneath Cyprus a fast anomaly is present in the S model that is absent in the P model. Another example is the deep slow P anomaly under the Ionian sea, which is also present in the S images, but with a weaker amplitude. The initial weighted variance is about the same for the P and S phase arrival time data. While Mediterranean S delays are larger than P delays (by a factor of about 3.1 (Schmid et al., 2004)), the measurement error for S arrivals is also larger by about the same factor. Since we scale the system of equations by the measurement error, the initial variances are similar for the P and S data sets. The variance reduction achieved is around ∼92% for the P data and ∼95% for the S data.

4.2. Joint P and S inversions

Before discussing the results of the combined P and S inversion, we show the results of several tests of the

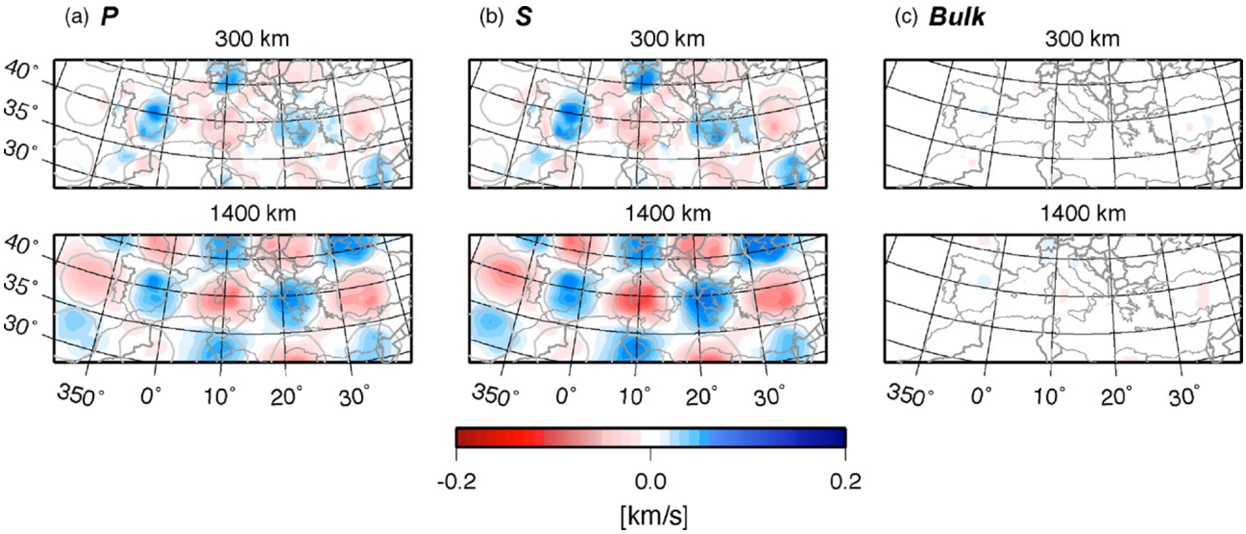

Fig. 3. Outcome of a resolution test for the combined *P* and *S* inversion. The input model only consists of shear velocity anomalies, no bulk sound anomalies are present.

data's resolving power. In addition to allowing an assessment of each data set's resolving power, the tests further demonstrates the strengths of a joint inversion of *S* and *P* data, as well as how strong the coupling is between shear and bulk sound heterogeneity. The tests also help us to choose appropriate values for weights and regularization parameters used in the inversion.

The resolving power for the following hypothetical models were tested:

- $\delta\beta \pm 0.2$ km/s and $\delta\Phi = 0$ km/s
- $\delta\beta$ and $\delta\Phi \pm 0.2$ km/s, $\delta\beta$ and $\delta\Phi$ correlated
- $\delta\beta \pm 0.2$ km/s and $\delta\Phi \pm 0.2$ km/s, $\delta\beta$ and $\delta\Phi$ anti-correlated

We use a harmonic input pattern. Fig. 3 shows the results of the first test, where the input pattern consists solely of shear velocity anomalies without the presence of bulk sound velocity anomalies. The amount of erroneous mapping of shear wave velocity anomalies into bulk sound velocity anomalies is small. In Fig. 4 we add a bulk sound velocity anomaly pattern of the same strength and location as that of the shear wave velocity anomalies. The resolution test shows that the anomaly

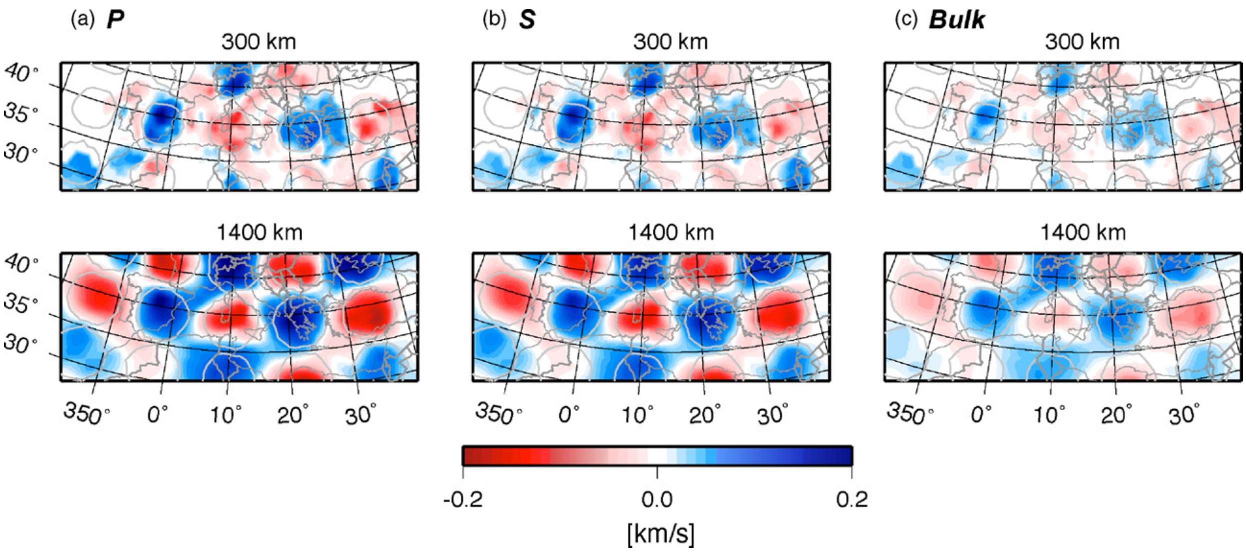

Fig. 4. Same as Fig. 3, except that bulk sound anomalies are now present as well in the input model. These are of the same strength as the shear velocity anomalies.

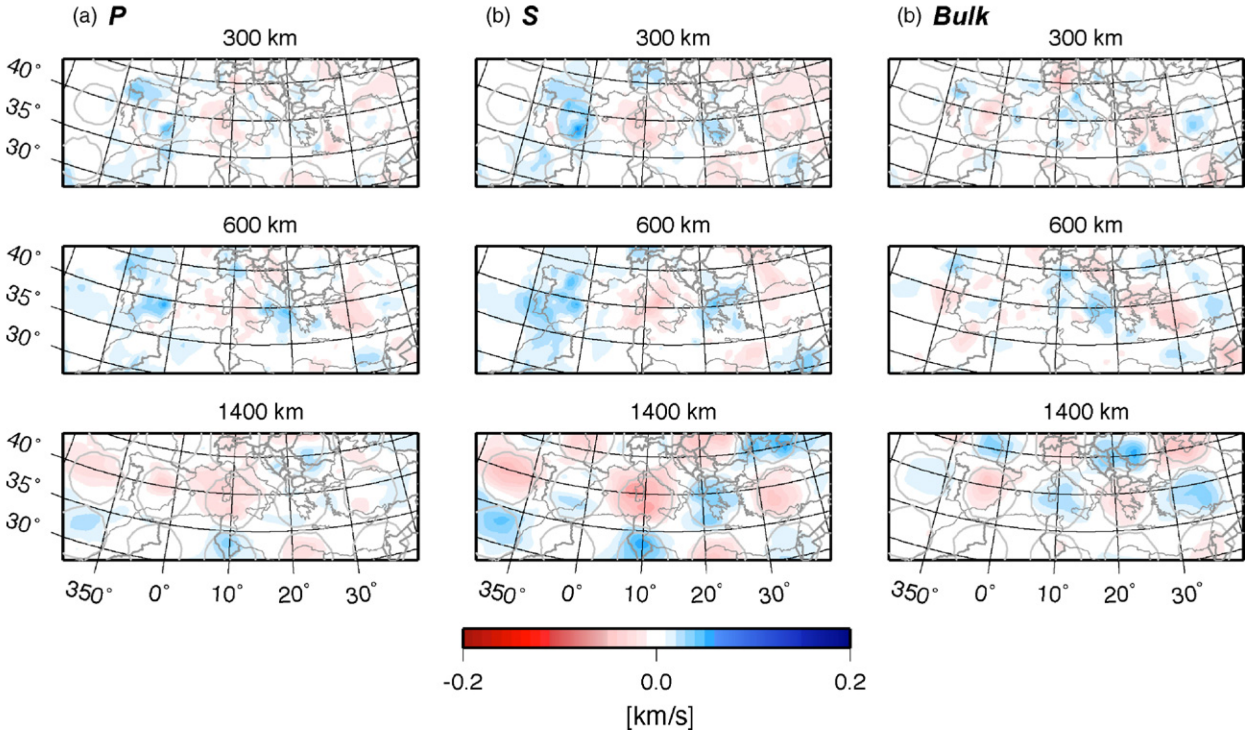

Fig. 5. Same as Fig. 4, shear velocity and bulk sound anomalies are again of the same strength but are anti-correlated, maxima in the shear velocity input pattern are co-located with bulk minima.

pattern is retrieved for both velocities, but the anomaly strength is better resolved for shear than for bulk heterogeneity. Finally, Fig. 5 shows the same test as in Fig. 4, except that the bulk velocity pattern that is input is anti-correlated with the shear velocity pattern. Even though the amplitudes of the recovered anomalies are strongly reduced compared to the correlated case, both patterns are resolved. However, the completely anti-correlated case is not realistic, because it predicts negligible P delay times (since $d\mu$ and dK would tend to cancel each other out), while we observe significant ones.

It is evident from these tests, that it is more difficult to resolve the velocity patterns if they are not correlated or even anti-correlated. Thus, with the given data, we lack the ability to reliably to resolve independent variations on small scales (100 km).

We use the following strategy to find the preferred joint P and S model. First we settled on a damping value for the shear component of our model through studying a series of inversions in which we suppressed anomalies in the bulk sound velocity. By looking at the trade-off curve between model-norm and variance reduction, the damping value for the shear velocity model was obtained. This results in a model where $\delta\Phi$ is basically zero and the P anomalies are simply a linear function of the S anomalies. This pure shear anomaly model results in a variance reduction slightly lower than in the individual inversions of P and S data. Thus, without taking into account perturbations in the bulk sound velocity, we can find a good fit to both data sets. We then settled on a damping value for the bulk component of our model by studying a series of inversions in which we allowed for shear and bulk sound velocity heterogeneity. The damping value for shear velocity anomalies was fixed to the value obtained from the preferred pure shear velocity model. Again, we choose the damping (for bulk sound anomalies) for the preferred model in such a manner that the trade-off between data fit and model norm is optimized (see Fig. 6). Then, fixing the value of bulk sound damping to the one found in this series of inversions, we ran another series where we again varied shear velocity damping. However, we found that the preferred value of shear velocity damping needs not to be readjusted. It turns out that we can apply higher values of damping for bulk sound velocities than what is needed for shear wave velocities.

Variance reduction is about the same as in the individual inversions. Note that the applied smoothness regu-

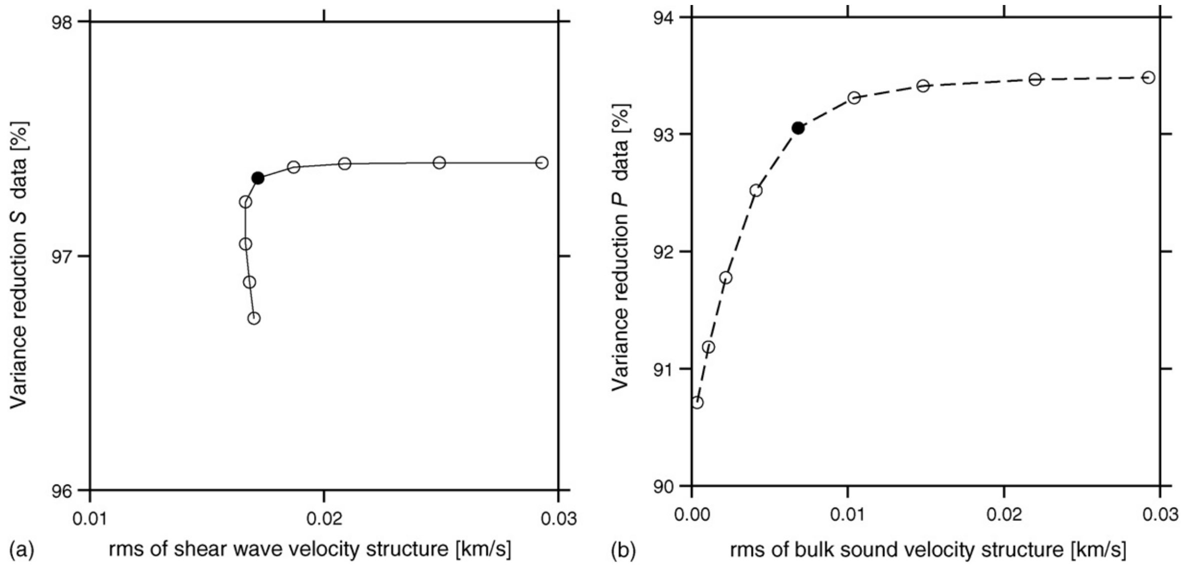

Fig. 6. Root mean square (rms) vs. variance reduction for different values of damping for the bulk sound velocity for: (a) *S* data and shear velocity structure and (b) *P* data and bulk sound velocity structure. Shear velocity damping is kept constant (at 2), black dots give the preferred model (bulk sound damping at 8). Using lower values for bulk damping (to the right of the black dots) gives a larger rms without no improvement in data fit, while using higher values for damping lead to a decreased data fit.

larization in the combined model is of the same strength as in the individual inversions. Fig. 7 shows the model that we obtained without including the regional waveform data. The preferred model further includes this data set and depth sections are shown in Fig. 8 while cross-sections are shown in Fig. 9. While the overall resolving power improves through inclusion of the regional waveform data, we verified that the main conclusions do not

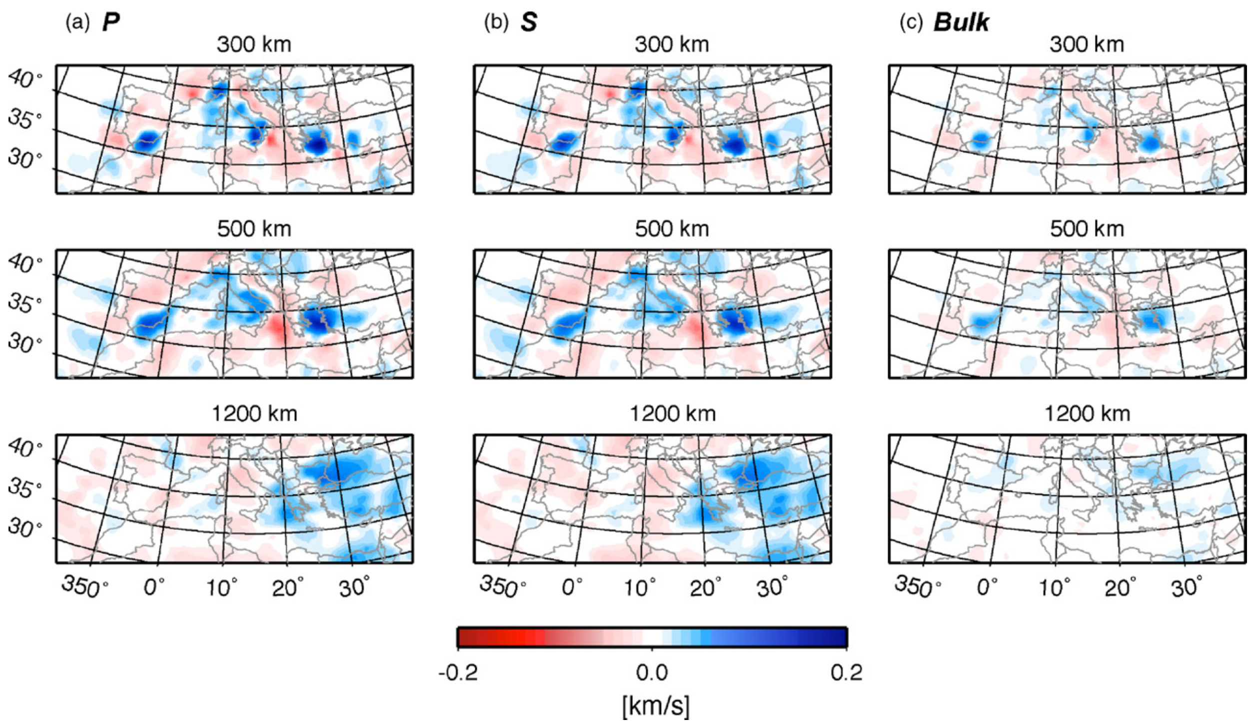

Fig. 7. Depth sections of the preferred joint model without usage of the regional waveform data.

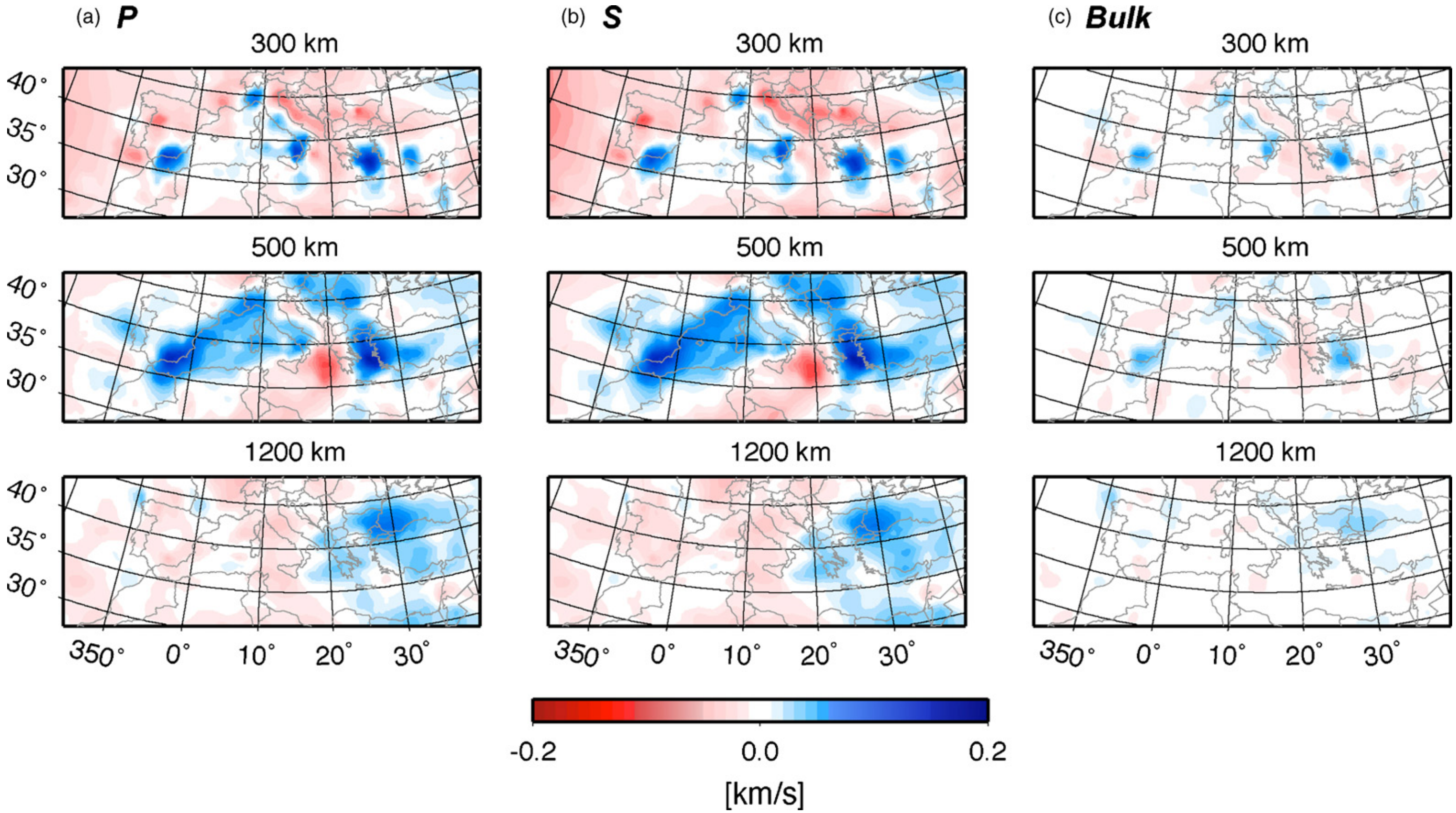

Fig. 8. Depth sections of the preferred joint model, regional waveform data are included.

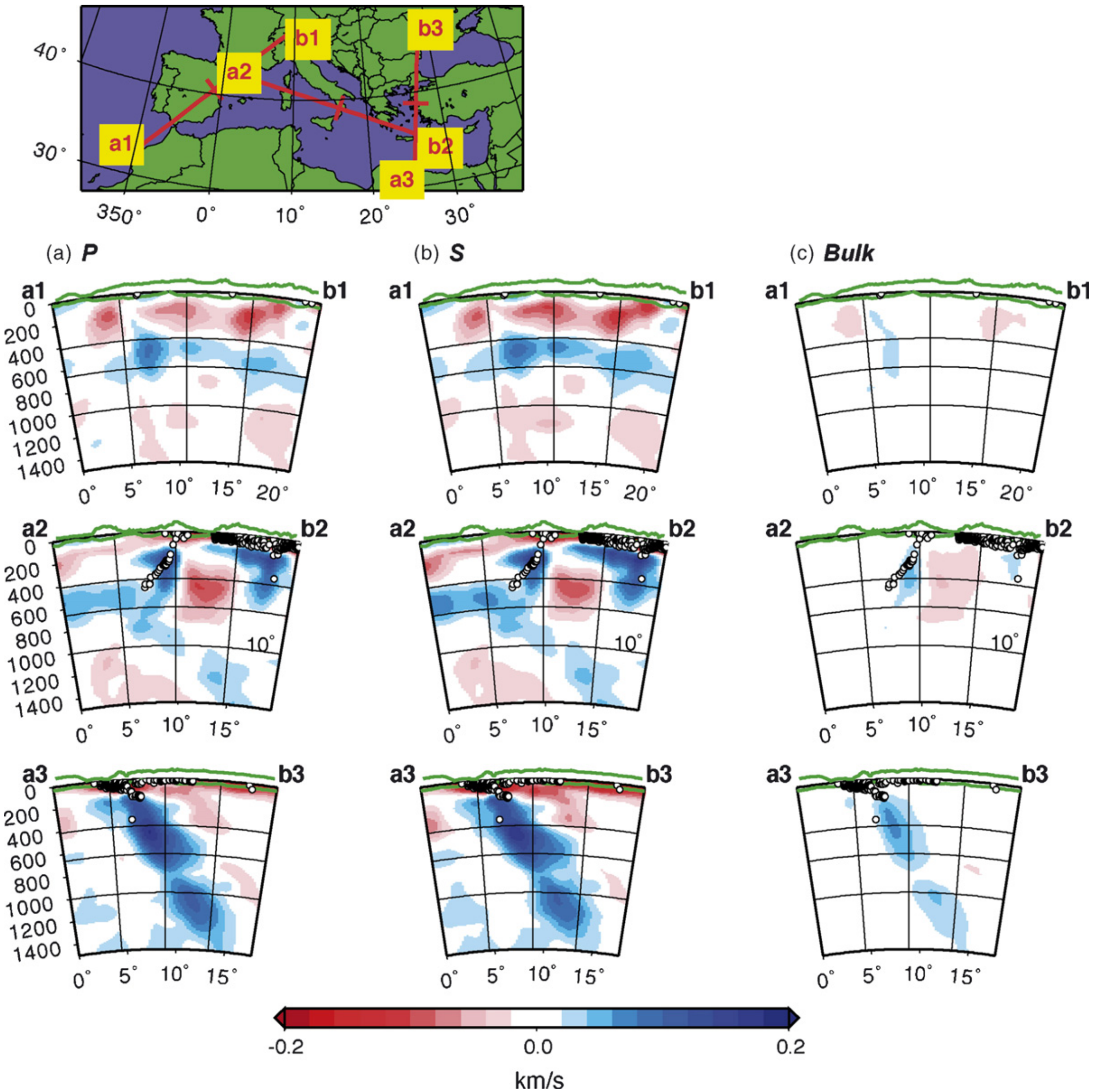

Fig. 9. Cross-section through the preferred joint model, regional waveform data are included.

depend on their inclusion and are thus unrelated to data coverage issues.

The large scale *P* and *S* velocity heterogeneity obtained from the joint inversion (Figs. 7 and 8) is very similar to that derived in individual inversions (Fig. 1). At smaller scales, some differences become apparent. For example, the slow anomaly south-east of Sicily appears much weaker in the images from *S* phase arrival time data than in the *P* images. Yet when jointly inverting the combined data-set, it also appears in the shear wave velocity images. Thus, this feature was only badly resolved by the teleseismic arrival time data of *S*, perhaps because of wavefront healing after passage through the low-velocity anomaly. A feature that is absent in the combined inversion is the slow anomaly seen in the *S* teleseismic arrival time image beneath Spain from 500 to 650 km. On the other hand, the fast material seen in the *S* image at 650 km beneath Cyprus and the northeasternmost corner of the Mediterranean sea still shows up in the combined inversion. However at 300 km, the combined inversion is closer to the *P* image and the anomaly is less broad than in the *S* image.

As mentioned above, already without allowing for bulk sound heterogeneity, an acceptable fit to the data is possible. So it is no surprise that the preferred joint *P* and *S* model requires merely small bulk sound velocity anomalies.

Because they appear to be relatively small, bulk sound velocity anomalies are harder to detect than shear-wave velocity anomalies. Furthermore, bulk sound velocity is not a quantity for which independent data exist and whatever we infer about its structure is affected by the trade-off with shear velocity. Thus, by placing firmer bounds on anomalous shear structure we reduce this trade-off and thus better constrain anomalous bulk sound structure. We better constrain shear structure through the joint inversion of teleseismic arrival times, regional body and surface wave forms, and Moho depth.

5. Discussion

The model we obtained shows well-known features such as the Hellenic and the Calabrian subduction zones. These have been extensively discussed in earlier tomographic studies (e.g. Spakman et al. (1993), Piromallo and Morelli (2003), Marone et al. (2004), Schmid et al. (2006)), thus we focus our discussion on the relation between bulk sound and shear wave velocity perturbations.

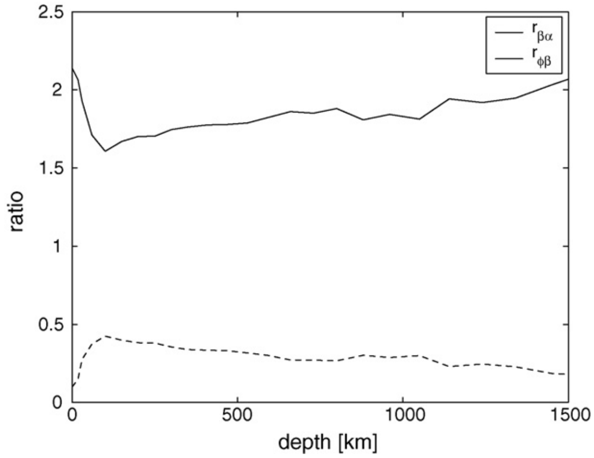

Fig. 10. Layer averages of the ratios given in Eq. (14) (dashed line) and Eq. (13) (solid line).

In order to quantify their contributions, we calculate the bulk sound to shear wave velocity heterogeneity,

$$r_{\Phi\beta} = \frac{\delta\Phi/\Phi_0}{\delta\beta/\beta_0} = \frac{\delta\ \ln \Phi}{\delta\ \ln \beta} \tag{13}$$

and the shear wave to compressional wave velocity heterogeneity,

$$r_{\beta\alpha} = \frac{\delta\beta/\beta_0}{\delta\alpha/\alpha_0} = \frac{\delta\ \ln \beta}{\delta\ \ln \alpha} \tag{14}$$

These ratios allow to draw some conclusions on the underlying cause of an anomaly, e.g. whether it is of thermal or compositional origin. Fig. 10 shows the layer averages of these quantities. $r_{\beta\alpha}$ is around 1.8 in the uppermost 1000 km and appears to increase to about 2.2 below 1200 km. These values of $r_{\beta\alpha}$ are in good agreement to those given in Masters et al. (2000), Kennett and Gorbatov (2004), Su and Dziewonski (1997).

$r_{\Phi\beta}$ varies between 0.2 and 0.4, higher values in the upper parts of the model. The strength of the bulk sound anomalies appears to decrease with depth, and *P* anomalies can thus be explained predominantly by variations in the shear wave velocity. No evidence is found for large scale anti-correlation between bulk sound and shear wave velocity variations, and the regions where $r_{\Phi\beta}$ is large, are restricted to zones of poor ray coverage. However, the observed values of the average ratio of $r_{\Phi\beta}$ may be biased by the abundance of fast anomalies and may thus not be valid for slow anomalies. Indeed, the slow shear wave velocity feature south-east of Sicily, finds only little expression as a bulk sound anomaly. However, a synthetic test (Fig. 11) indicates that due

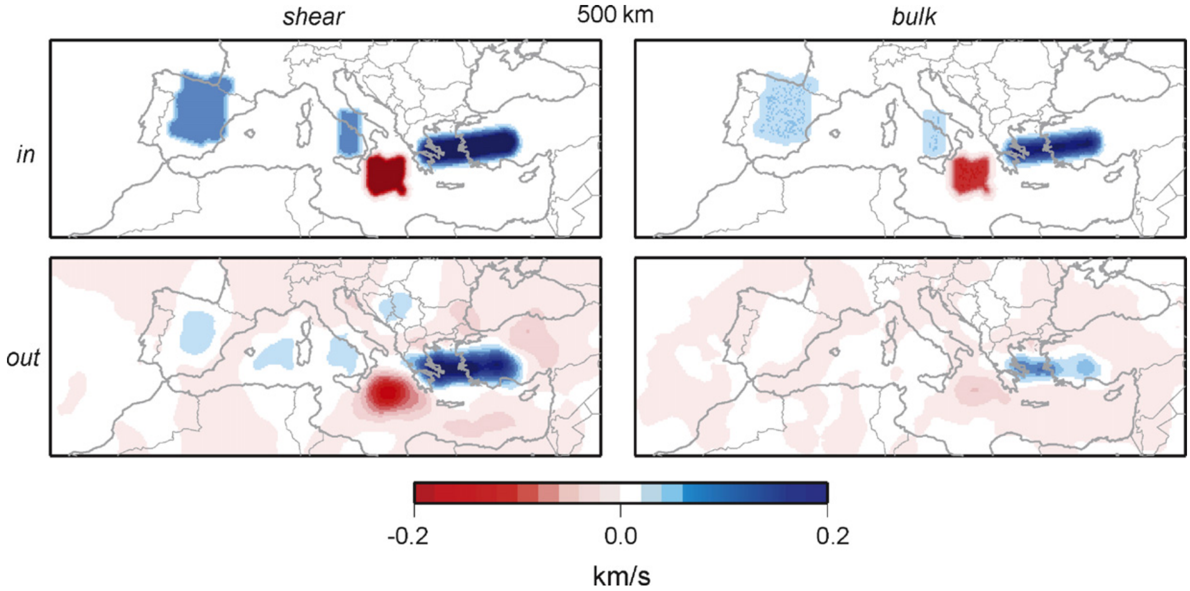

Fig. 11. Resolution test with a realistic input model. Top row shows the input model, the result is shown in the bottom row. Shear wave and bulk sound velocity structure are identical, except that the amplitudes of the latter are reduced by a factor of 2, corresponding to an $r_{\Phi\beta}$ of about ∼0.4.

to its small amplitude, the bulk sound anomaly is on the brink of being resolvable. Thus, the absence of this low velocity anomaly in the bulk sound velocity is not significant.

Although we cannot exclude compositional heterogeneity playing a role in this region, the observed anomalies are well in agreement with a predominantly thermal cause. Cammarano et al. (2003) list the temperature sensitivities of α, β and Φ. They obtained the values by forward calculating seismic velocity as a function of pressure and temperature for various compositions using anharmonic data for each mineral phase. They also include the important effect of anelasticity (Karato, 1993). The temperature sensitivity (in % velocity perturbation per Kelvin) of shear wave velocity is about twice as large as the sensitivity of compressional wave velocity, which in turn is again twice as large as that for the bulk sound velocity. The highest values that we observe for $d\ln\alpha$ are around 2% and 1.5% at depths of 400 and 650 km, respectively. The percentage values for $d\ln\beta$ are about twice as large (4% and 3%) at these depths, while those for Φ are around 1% and less. Using the values given by Cammarano et al. (2003) for the 1300 °C adiabat, these perturbations correspond to temperatures around 300–400 K cooler than the adiabat. The low velocity anomaly southeast of Sicily has somewhat smaller amplitudes, that correspond to temperatures about 200 K warmer than the surrounding mantle.

6. Conclusions and discussion

P and *S* velocity variations have similar patterns beneath the Mediterranean region. Least-structure models for bulk sound and shear wave velocity heterogeneity show that bulk and shear anomalies are correlated down to 1400 km and that significant bulk sound velocity anomalies are not required by the data. The correlation and proportion between shear and bulk heterogeneity in the least-structure models indicates that the simplest (least-structure) explanation of our data agrees with an origin that is dominantly but not necessarily exclusively thermal in nature.

The transition zone beneath the Mediterranean region appears to be 300–400 K cooler than the global average, with the exception of that beneath the Ionian sea, which could be up to 200 K warmer. The joint inversion of *P* and *S* data allows for a better resolved model than individual inversions can achieve.

Acknowledgments

We are grateful for constructive reviews from two anonymous reviewers. We thank John VanDecar for numerous insightful discussions as well as constructive review comments. CS and the MIDSEA data acquisition effort were supported by the Swiss Nationalfonds. SvdL gratefully acknowledges support from US DOE contract DE-FC52-04NA25541. We also thank the Carnegie

Institution of Washington for supporting the initial development of the new, joint inversion method applied here. This work would not have been accomplished without the data acquisition efforts of the MIDSEA participants (see Van der Lee et al. (2001) for a full list). This is contribution number 1459 of the Institute of Geophysics, ETH Zürich.

References

Antolik, M., Gu, Y.J., Ektsröm, G., Dziewonski, A.M., 2003. J362D28: a new joint model of compressional and shear velocity in the Earth's mantle. Geophys. J. Int. 153, 443–466.

Bijwaard, H., 1999. Seismic travel-time tomography for detailed global mantle structure, Ph.D. Thesis, University of Utrecht.

Cammarano, F., Goes, S., Vacher, P., Giardini, D., 2003. Inferring upper mantle temperatures from seismic velocities. Phys. Earth Planet. Int. 138, 197–222.

Dercourt, J., Zonenshain, L., Ricou, L., Kazmin, V., Le Pichon, X., Knipper, A., Grandjacquet, C., Sbortshikov, I., Geyssant, J., Lepvrier, C., Pechersky, D., Boulin, J., Sibuet, J., Savostin, L., Sorokhtin, O., Westphal, M., Bazhenov, M., Lauer, J., Biju-Duval, B., 1986. Geological evolution of the Tethys Belt from the Atlantic to the Pamirs since the Lias. Tectonophysics 123, 241–315.

Gorbatov, A., Kennett, B.L.N., 2003. Joint bulk-sound and shear tomography for Western Pacific subduction zones. Earth Planet. Sci. Lett. 210, 527–543.

Karato, S., 1993. Importance of anelasticity in the interpretation of seismic tomography. Geophys. Res. Lett. 20, 1623–1626.

Kennett, B.L.N., Engdahl, E.R., 1991. Traveltimes for global earthquake location and phase identification. Geophys. J. Int. 105, 429–465.

Kennett, B.L.N., Gorbatov, A., 2004. Seismic heterogeneity in the mantle-strong shear wave signature of slabs from joint tomography. Phys. Earth Planet. Int. 146, 87–100.

Kennett, B.L.N., Widiyantoro, S., van der Hilst, R.D., 1998. Joint seismic tomography for bulk sound and shear wave speed in the Earth's mantle. J. Geophys. Res. 103, 12469–12493.

Marone, F., van der Meijde, M., van der Lee, S., Giardini, D., 2003. Joint inversion of local, regional and teleseismic data for crustal thickness in the Eurasia-Africa plate boundary region. Geophys. J. Int. 154, 499–514.

Marone, F., van der Lee, S., Giardini, D., 2004. Three-dimensional upper-mantle *S*-velocity model for the Eurasia-Africa plate boundary region. Geophys. J. Int. 158, 109–130.

Masters, G., Laske, G., Bolton, H., Dziewonski, A., 2000. The relative behaviour of shear velocity, bulk sound speed, and compressional velocity in the mantle: implications for chemical and thermal strcuture, Earth's deep interior: mineral physics and tomography from the atomic to the global scale, AGU Geophysical Monograph 117, pp. 63–87.

Panza, G., Mueller, S., Calcagnile, G., 1980. The gross features of the lithosphere–asthenosphere system in Europe from seismic surface waves and body waves. Pure Appl. Geophys. 118, 1209–1213.

Pasyanos, M., Walter, W., 2002. Crust and upper mantle structure of North Africa, Europe, and the Middle East from inversion of surface waves. Geophys. J. Int. 149, 464–482.

Piromallo, C., Morelli, A., 2003. *P* wave tomography of the mantle under the Alpine-Mediterranean area, J. Geophys. Res., 108, 2065, doi:10.1029/2002JB001,757.

Schmid, C., van der Lee, S., Giardini, D., 2004. Delay times and shear wave splitting in the Mediterranean region. Geophys. J. Int. 159, 275–290.

Schmid, C., van der Lee, S., VanDeacar, J.C., Engdahl, E.R., Giardini, D., 2006. Three-dimensional *S*-velocity of the mantle in the Africa-Eurasia plate boundary region from phase arrival times and regional waveforms, J. Geophys. Res., submitted for publication.

Spakman, W., van der Lee, S., van der Hilst, R.D., 1993. Travel-time tomography of the European-Mediterranean mantle down to 1400 km. Phys. Earth Planet. Int. 79, 3–74.

Stampfli, G.M., Borel, G.D., 2002. A plate tectonic model for the Paleozoic and Mesozoic constrained by dynamic plate boundaries and restored synthetic oceanic isochrons. Earth Planet. Sci. Lett. 196, 17–33.

Su, W., Dziewonski, A.M., 1997. Simultaneous inversion for 3D variations in shear and bulk velocity in the mantle. Phys. Earth Planet. Sci. Int. 100, 135–156.

Van der Lee, S., Nolet, G., 1997. Upper mantle *S* velocity structure of North America. J. Geophys. Res. 102, 22815–22838.

Van der Lee, S., Marone, F., van der Meijde, M., Giardini, D., Deschamps, A., Margheriti, L., Burkett, P., Soloman, S.C., Alves, P.M., Chouliaras, M., Eshwehdi, A., Suleiman, A., Gashut, H., Herak, M., Ortiz, R., Davila, J.M., Ugalde, A., Vila, J., Yelles, K., 2001. Eurasia-Africa plate boundary region yields new seismographic data. Eos Trans. AGU 82 (51), 637–646.

VanDecar, J.C., 1991. Upper-mantle structure of the Cascadia subduction zone from non-linear teleseismic travel-time inversion, Ph.D. Thesis, University of Washington, Seattle.

VanDecar, J.C., Crosson, R.S., 1990. Determination of teleseismic relative phase arrival times using multi-channel cross-correlation and least-squares. Bull. Seismol. Soc. Am. 80, 150–169.

Zielhuis, A., Nolet, G., 1994. Shear-wave velocity variations in the upper mantle beneath central Europe. Geophys. J. Int. 117, 695–715.